ORNL/TM-2017/377

Fracture Toughness Evaluation of Select Advanced Replacement Alloys for LWR Core Internals

Xiang Chen
Lizhen Tan

August 25, 2017

OAK RIDGE NATIONAL LABORATORY
MANAGED BY UT-BATTELLE FOR THE US DEPARTMENT OF ENERGY

ORNL/TM-2017/377

Light Water Reactor Sustainability (LWRS) Program
M2LW-17OR0406024

FRACTURE TOUGHNESS EVALUATION OF SELECT ADVANCED REPLACEMENT ALLOYS FOR LWR CORE INTERNALS

Xiang Chen and Lizhen Tan
Materials Science and Technology Division
Oak Ridge National Laboratory

Date Published: August 25, 2017

Prepared under the direction of the
U.S. Department of Energy
Office of Nuclear Energy
Light Water Reactor Sustainability
Materials Aging and Degradation Pathway

Prepared by
OAK RIDGE NATIONAL LABORATORY
Oak Ridge, Tennessee 37831-6283
managed by
UT-BATTELLE, LLC
for the
US DEPARTMENT OF ENERGY
under contract DE-AC05-00OR22725

CONTENTS

Page

LIST OF FIGURES

Figure **Page**

LIST OF TABLES

Table **Page**

ACKNOWLEDGMENTS

This research was sponsored by the U.S. Department of Energy, Office of Nuclear Energy, Light Water Reactor Sustainability Program under contract DE-AC05-00OR22725 with UT-Battelle, LLC/Oak Ridge National Laboratory. The authors wish to thank Dr. Keith Leonard who provided support for this work, and to Eric Manneschmidt and Ron Swain for helping the tests. The authors are also grateful for the many helpful discussions with Drs. Mikhail Sokolov, Raj Pathania (EPRI), Larry Nelson (JLN Consulting), G.S. Was [University of Michigan (UM)], M. Wang (UM) and M. Song (UM). Dr. Maxim Gussev is appreciated for reviewing the report.

EXECUTIVE SUMMARY

Life extension of the existing nuclear reactors imposes irradiation of high fluences to structural materials, resulting in significant challenges to the traditional reactor materials such as type 304 and 316 stainless steels. Advanced alloys with superior radiation resistance will increase safety margins, design flexibility, and economics for not only the life extension of the existing fleet but also new builds with advanced reactor designs. The Electric Power Research Institute (EPRI) teamed up with Department of Energy (DOE) to initiate the Advanced Radiation Resistant Materials (ARRM) program, aiming to develop and test degradation resistant alloys from current commercial alloy specifications by 2021 to a new advanced alloy with superior degradation resistance in light water reactor (LWR)-relevant environments by 2024.

Fracture toughness is one of the key engineering properties required for core internal materials. Together with other properties, which are being examined such as high-temperature steam oxidation resistance, radiation hardening, and irradiation-assisted stress corrosion cracking resistance, the alloys will be down-selected for neutron irradiation study and comprehensive post-irradiation examinations.

According to the candidate alloys selected under the ARRM program, ductile fracture toughness of eight alloys was evaluated at room temperature and the LWR-relevant temperatures. The tested alloys include two ferritic alloys (Grade 92 and an oxide-dispersion-strengthened alloy 14YWT), two austenitic stainless steels (316L and 310), four Ni-base superalloys (718A, 725, 690, and X750). Alloy 316L and X750 are included as reference alloys for low- and high-strength alloys, respectively. Compact tension specimens in 0.25T and 0.2T were machined from the alloys in the T-L and R-L orientations according to the product forms of the alloys. This report summarizes the final results of the specimens tested and analyzed per ASTM Standard E1820.

Unlike the ferritic alloys showing slight decreases (Grade 92) or significant decreases (14YWT) in fracture toughness at elevated temperatures, the fracture toughness of the austenitic stainless steels and Ni-base superalloys were not strongly dependent upon the test temperatures. The fracture toughness of the alloys at the LWR-relevant temperatures was estimated by averaging the toughness values within 250–350°C, which suggested the fracture toughness of the alloys in a descending order as 316L (752±98 MPa√m), 310 (513±66 MPa√m), 718A (313±43 MPa√m), 690 (267±48 MPa√m), 725 (218±55 MPa√m), X750 (145±16 MPa√m), Grade 92 (112±12 MPa√m), and 14YWT (63±3 MPa√m).

Tearing modulus of the alloys was analyzed in the meantime, which were not strongly dependent upon the test temperatures. The high-strength alloys 718A, 725, X750, and 14YWT had the lowest tearing modulus, ranging from ~45 to ~7. Alloy 690 exhibited the highest tearing modulus on the order of 450, followed by 316L and 310 on the order of 260. Grade 92 had a noticeably lower tearing modulus on the order of 70.

1. INTRODUCTION

Nuclear power currently provides a significant fraction of the United States' non-carbon emitting power generation. In future years, nuclear power must continue to generate a significant portion of the nation's electricity to meet the growing electricity demand, clean energy goals, and to ensure energy independence. New reactors will be an essential part of the expansion of nuclear power. However, given limits on new builds imposed by economics and industrial capacity, the extended service of the existing fleets will also be required.

Nuclear reactors present a very harsh environment for components service. Components within a reactor core must tolerate high temperatures, water, stress, vibration, and an intense neutron field. With the nominal irradiation temperature of ~290°C in light water reactors (LWRs), actual component temperatures range from 270°C to 370°C depending on the relative position of the component within the reactor core and relative amounts of cooling and gamma heating. Degradation of materials in this environment can lead to reduced performance, and in some cases, sudden failure.

Extending the service life of a reactor will increase the total neutron fluence to each component and may result in radiation-induced effects not yet observed in LWR conditions, although this form of degradation has been observed in fast reactor conditions. Radiation-induced processes must be carefully considered for higher fluences, particularly the influence of radiation-induced segregation (RIS), swelling, and/or precipitation on embrittlement. Neutron irradiation field can produce large property and dimensional changes in materials. For LWRs, high-temperature embrittlement and creep are not common problems due to the lower reactor temperature. However, radiation embrittlement, phase transformation, segregation, and swelling have all been observed in reactor components. Increases in neutron fluence may exacerbate radiation-induced or -enhanced microstructural and property changes. Comprehensive reviews on radiation effects on the traditional structural materials of LWRs can be found in Ref. [1,2,3].

It is desirable to have advanced alloys that possess greater radiation resistance than the traditional reactor materials. The use of such advanced alloys in replacing the traditional reactor materials for the extension of the existing fleets and the building of new reactors will bring improved safety margins and economics. To identify and develop advanced radiation resistant materials, Electric Power Research Institute (EPRI) has partnered with Department of Energy (DOE) Light Water Reactor Sustainability Program to conduct an Advanced Radiation Resistant Materials (ARRM) program. The EPRI report of "Critical Issues Report and Roadmap for the Advanced Radiation-Resistant Materials Program" [4] reviewed the current commercial and advanced alloys that are applicable as core structural materials of LWRs and laid out a detailed research plan to meet the goal of the program.

Fracture toughness is one of the basic properties required to be screened for the select advanced alloys. Together with other properties such as high-temperature steam oxidation resistance, radiation hardening, and irradiation-assisted stress corrosion cracking resistance, the alloys will be down-selected for neutron irradiation study and comprehensive post-irradiation examinations to understand key factors governing superior properties, from which advanced replacement alloys will be developed and recommended for applications in LWR core internals. This report presents the testing results of fracture toughness of select advanced replacement alloys.

2. MATERIALS AND TEST CONDITIONS

2.1 Materials

Table 1 lists eight select alloys for fracture toughness tests, which includes their nominal compositions in weight percentages, heat numbers, product forms, and vendors or producers. The materials were examined to ensure acceptable chemistry homogeneity and microstructural uniformity. According to the type of the materials, they are classified as ferritic steels with a body-centered-cubic (bcc) crystal structure, austenitic stainless steels and nickel-base superalloys with a face-centered-cubic (fcc) crystal structure.

Table 1. Select advanced replacement alloys for fracture toughness tests

Category	Alloy	Nominal composition	Heat number	Product form	Vendor/Producer
Ferritic (bcc)	Grade 92	Fe–9Cr–1.8W–0.5MoVNb	011448	1.7”-thick Plate	Carpenter
	14YWT*	Fe–14Cr–3W–TiYO	FCRD-NFA1	0.3”-thick Plate	ORNL
Austenitic (fcc)	316L[a]	Fe–16Cr–10Ni–2Mo	857115	5.25”-diameter Bar	Outokumpu
	310	Fe–25Cr–20Ni	011509	1.75”-diameter Bar	Carpenter
Ni-base (fcc)	718A*	53Ni–20Cr–17Fe–5.2Nb–3MoTiAl	399	0.6”-thick Plate	Carpenter
	725*	58Ni–22Cr–8Mo–8Fe–4NbTi	416408	7”-diameter Bar	Carpenter
	690	60Ni–30Cr–10Fe	NX7075HK11	2.2”-thick Plate	Huntington
	X750*,[a]	71Ni–16Cr–8Fe–2.6TiNbAl	418365	6”-diameter Bar	Carpenter

* High-strength alloys
[a] Reference alloys

The tests involve two ferritic steels, including Grade 92 (a 9Cr ferritic-martensitic steel) and 14YWT [a 14Cr oxide-dispersion-strengthened (ODS) ferritic steel], two austenitic stainless steels, including 316L and 310, and four Ni-base superalloys, including 718, 725, 690 and X-750. According to their strength, high-strength alloys include X-750, 725, 718 and 14YWT. The other alloys belong to low-strength alloys. Alloy X-750 and 316L are used as reference alloys for the high- and low-strength alloys, respectively.

There were seven other alloys selected in screening tests, which include 439 (Fe–18Cr), 800 (Fe–20Cr–32Ni–TiAl), C22 (58Ni–22Cr–14Mo–3W–3Fe), 625 (61Ni–22Cr–9Mo–4Nb–4Fe), 625 direct aging, 625-plus (625+Ti), and Zr–2.5Nb. They are not included in this test matrix because of the observations of some poor performance, e.g., room temperature ductile brittle transition temperature of alloy 439 [5], poor resistance to irradiation-assisted stress corrosion cracking in alloys 800, 625, 625 direct aging and 625-plus [6], the greatest radiation hardening and poorest resistance to high-temperature steam oxidation of alloy C22 within the Ni-base superalloys [6,7], and the concern of severe accident conditions of Zr–2.5Nb with the poorest resistance to high-temperature steam oxidation among all the select alloys [7].

2.2 Test Specimens and Conditions

To evaluate the performance of the alloys at LWR-relevant temperatures, fracture toughness tests were conducted in the ductile regime at temperatures of 250, 300 and 350°C, as well as room temperature for comparison. Compact tension specimens with sizes of 0.25T and 0.2T according to the specifications in Figure 1 and 2, respectively, were extracted from the procured materials using electric discharge machining. The austenitic stainless steels and Ni-base superalloys were machined into 0.25T specimens, while the ferritic steels were machined into 0.2T specimens because of the limited material’s dimension

of 14YWT. The limited material of alloy 718 yield only four specimens with one specimen per temperature, while seven specimens were extracted from the other alloys.

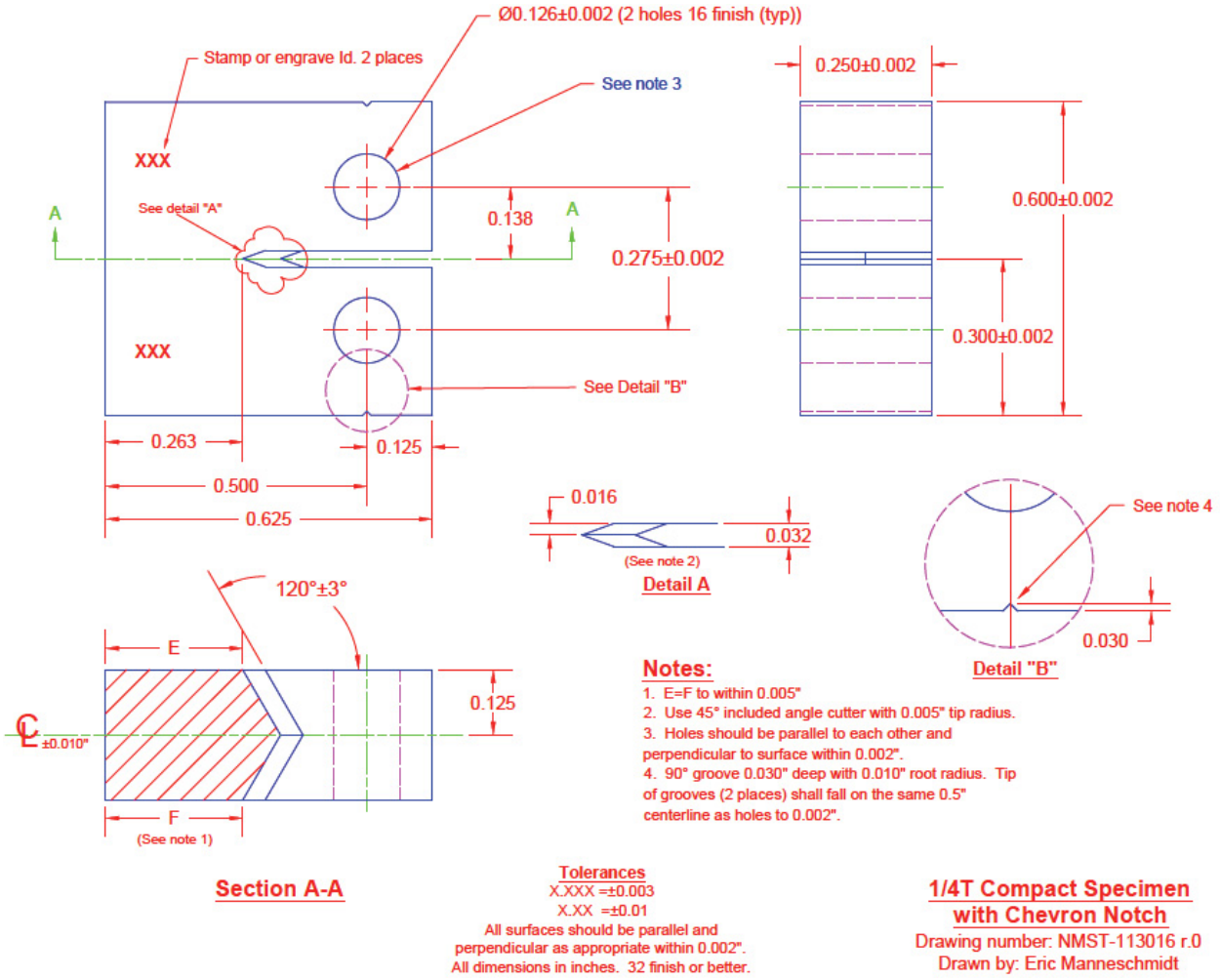

Figure 1. Specification of 0.25T compact specimen (dimensions are in inches).

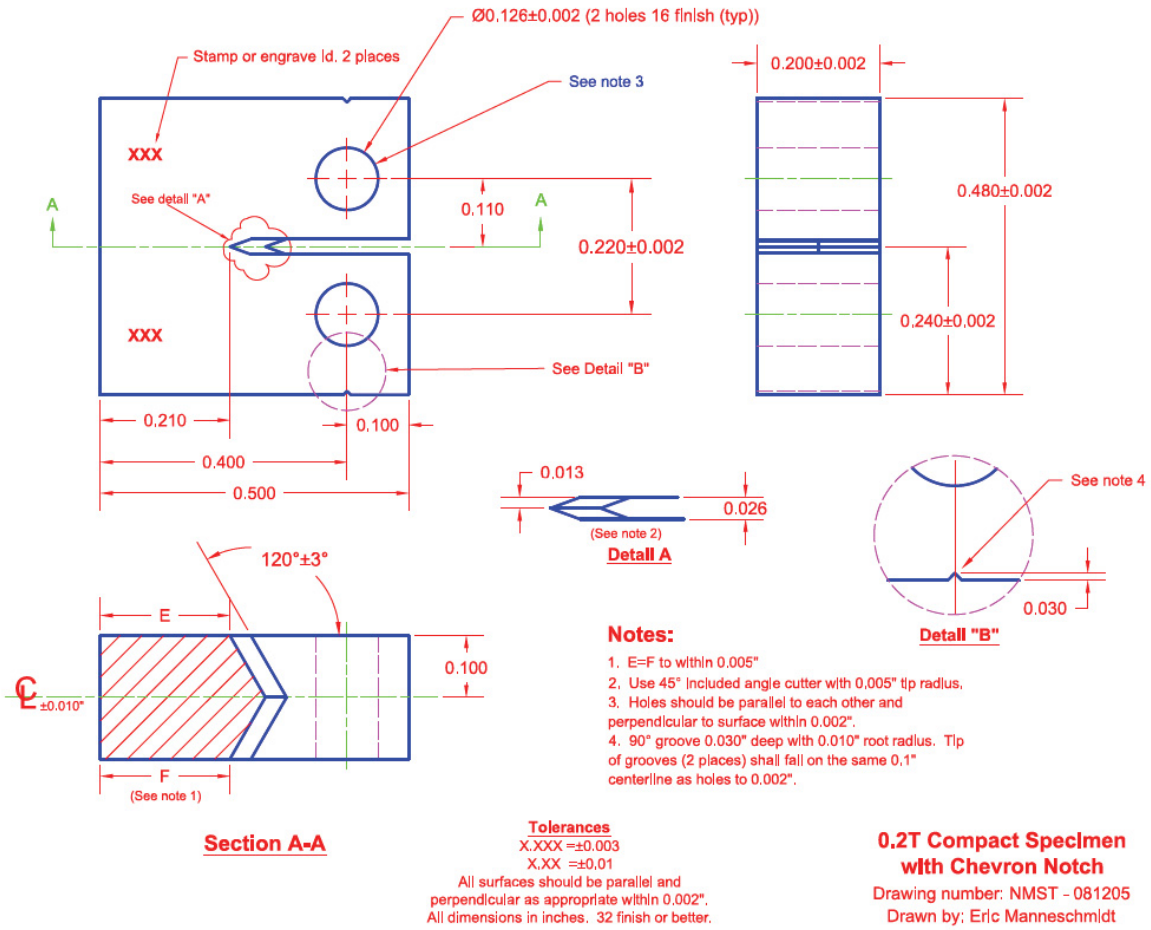

Figure 2. Specification of 0.2T compact specimen (dimensions are in inches).

The procured alloys were in plate or bar forms as listed in Table 1. According to the ASTM Standard E1823-13, "Standard Terminology Relating to Fatigue and Fracture Testing", the T-L and R-L specimen orientations, as shown in Figure 3, were extracted from the plate and bar forms, respectively. The T-L and R-L orientations are normally expected to reveal lower toughness values compared to the other orientations, which would provide conservative results for the alloys.

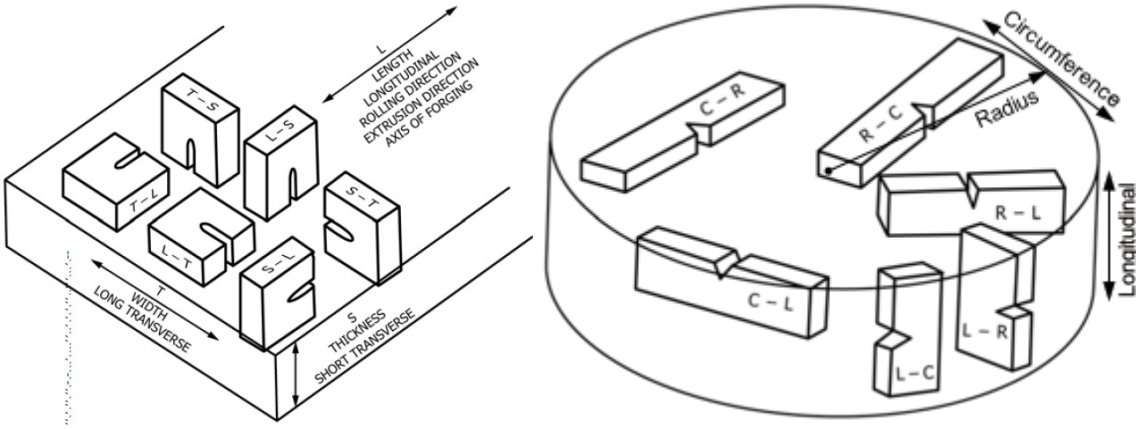

Figure 3. Crack plane orientation code for plate (left) and bar (right) [ASTM E1823-13].

Fracture toughness tests were conducted with a computer-controlled test and data acquisition system in general accordance with the ASTM Standard E1820, "Standard Test Method for Measurement of Fracture Toughness". The specimens were fatigue pre-cracked to a ratio of the crack length to specimen width (a/W) of about 0.5, and then side-grooved by 20% of their thickness (10% from each side) before testing. Specimens were tested in the laboratory on a 98-kN (22-kip) capacity servo-hydraulic machine. All tests were conducted in strain control, with an outboard clip gauge having a central flexural beam that was instrumented with four strain gauges in a full-bridge configuration.

2.3 Test and Analysis Methods

The specimens have been primarily tested and analyzed by the normalization method described in ASTM E1820 Annex 15 because of its time efficiency to deduce the results. In the case of specimens having toughness too high to be reliably analyzed by the normalization method, the conventional elastic unloading compliance (EUC) method was used. The normalization method only requires a load-displacement curve as in a tensile test with initial and final crack size measurements from the specimen fracture surface to determine the J-integral vs. crack growth resistance curve (J-R curve) according to the analytical procedures in ASTM E1820. In contract, the EUC method requires periodic unloading-reloading of the specimen to measure the specimen compliance (the ratio of the displacement increment to the load increment) which is used for calculating the real-time crack growth to derive the J-R curve. One example of the comparison of the load-displacement curves between the normalization method and the EUC method is given in Figure 4a. In a valid test, both methods can yield almost the same J-R curves as indicated in Figure 4b.

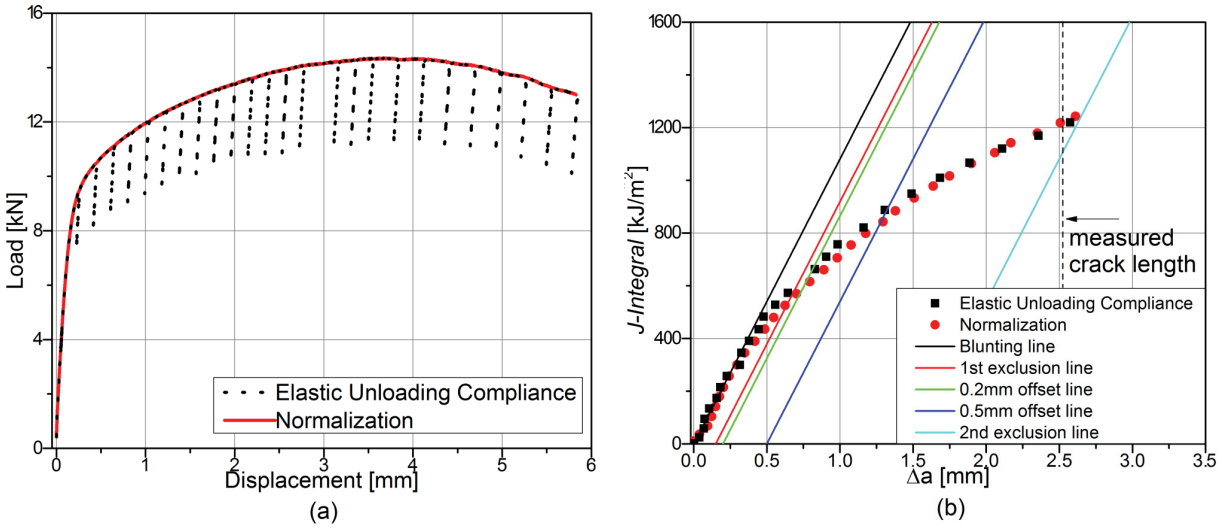

Figure 4. (a) EUC versus normalization load-displacement record for the J-R curve test; (b) comparison of J-R curves derived by EUC and normalization methods [8]

3. RESULTS AND DISCUSSIONS

3.1 J-R Curves

J-R curves of the fracture toughness tests in the ductile regime at room and elevated temperatures are shown in Figure 7, 6, and 7 for the ferritic alloys (Grade 92 and 14YWT), austenitic stainless steels (316L and 310), and Ni-base alloys (X750, 725, 718A and 690), respectively. The curves are plotted in scatter dots, representing each collected experimental data point. Unlike the majority specimens tested by the normalization method, showing generally continuous J-R curves, two specimens of 316L were tested at 23 and 350°C by the EUC method, with each data point in Figure 6a representing one unload-reloading sequence.

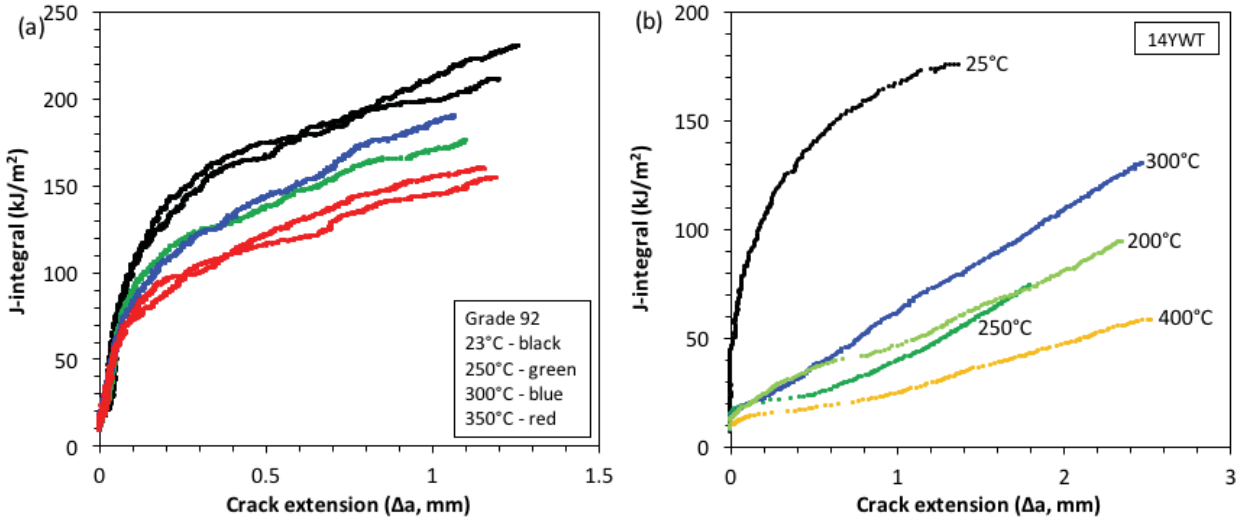

Figure 5. J-R curves of ferritic alloys (a) Grade 92 and (b) 14YWT [5], tested at room and elevated temperatures.

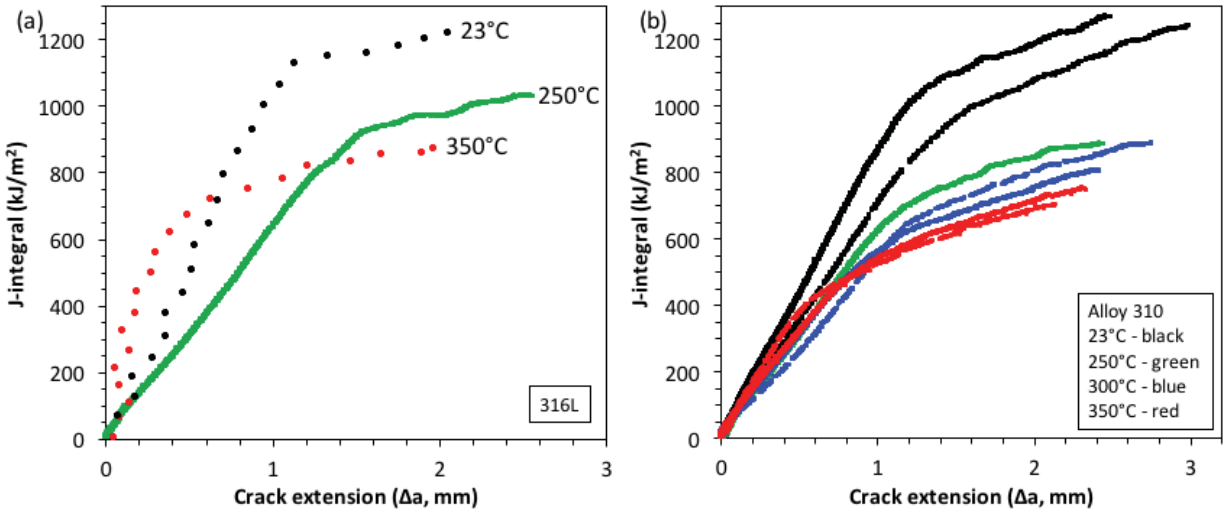

Figure 6. J-R curves of austenitic stainless steels (a) 316L and (d) 310, tested at room and elevated temperatures.

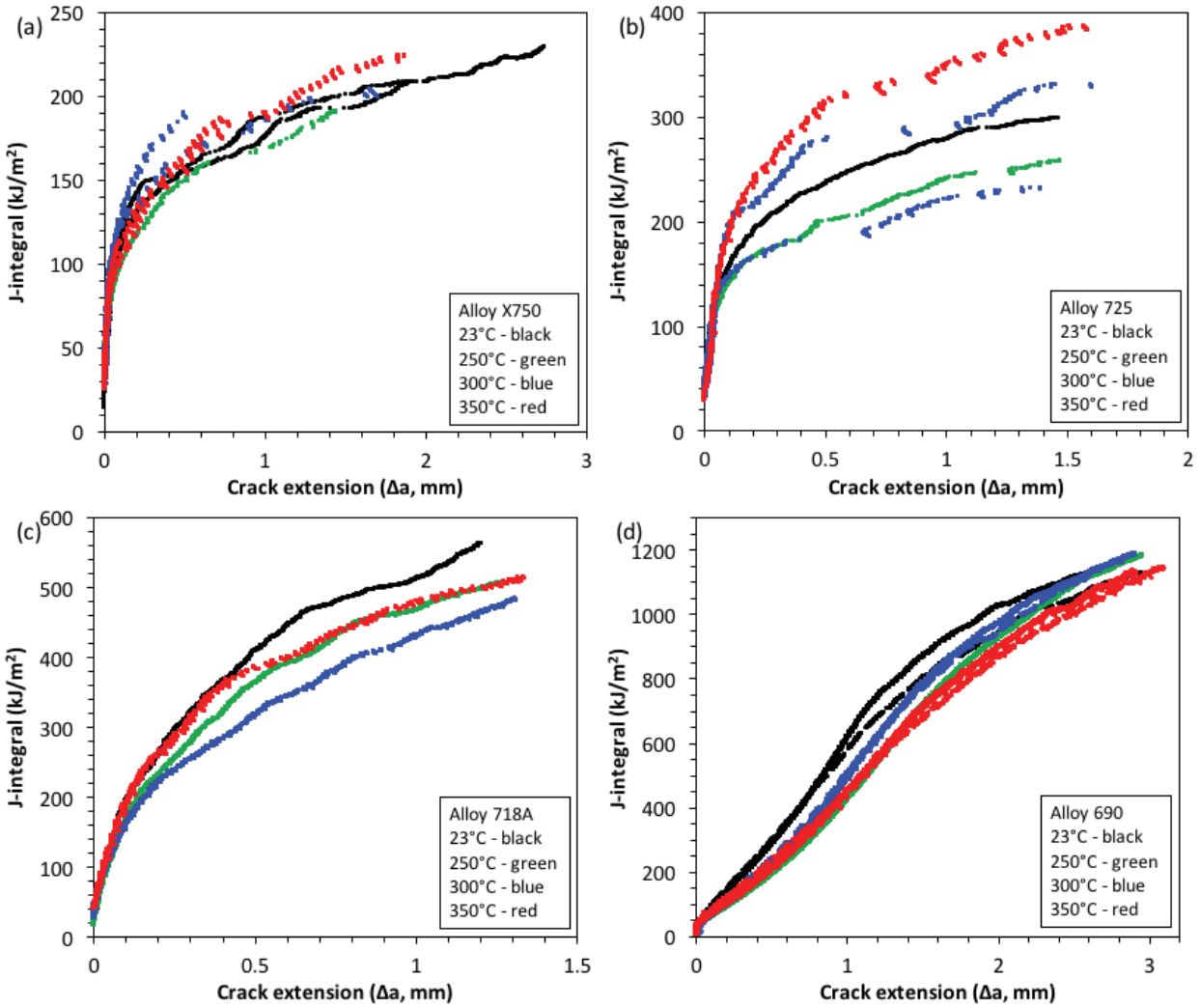

Figure 7. J-R curves of Ni-base alloys (a) X750, (b) 725, (c) 718A, and (d) 690, tested at room and elevated temperatures.

3.2 Fracture Toughness and Tearing Modulus

Values of *J*-integral at the onset of stable crack growth, J_Q, were converted to their equivalent values in terms of stress intensity K_{JQ} in MPa√m by the equation of $K_{JQ} = \sqrt{J_Q \frac{E}{1-\nu^2}}$, where E is Young's modulus and ν is Poisson ratio (= 0.3). The fracture toughness results of the eight alloys are plotted in Figure 8a with K_{JQ} in logarithmic scale as a function of the test temperatures. It should be noted that the specimens of alloys 316L, 310, and 690, except for the two data of alloy 690 at 250 and 350°C, did not completely comply with plane-strain conditions because of the high toughness of the three alloys and the small size of test specimens, which may result in somewhat higher fracture toughness test values. In general, the fracture toughness of the austenitic stainless steels and Ni-base alloys are not strongly dependent upon the test temperatures. The alloys exhibited approximately constant or slightly decreased fracture toughness at elevated temperatures. In contrast, ferritic alloys Grade 92 and 14YWT showed slight and significant decreases, respectively, in fracture toughness with increasing test temperatures. The fracture toughness of the alloys at the LWR-relevant temperatures (250–350°C) was estimated by

averaging the toughness values within the temperature range. Figure 8b shows the average fracture toughness with standard deviations of the alloys, which suggests the fracture toughness of the alloys in a descending order as 316L, 310, 718A, 690, 725, X750, Grade 92, and 14YWT.

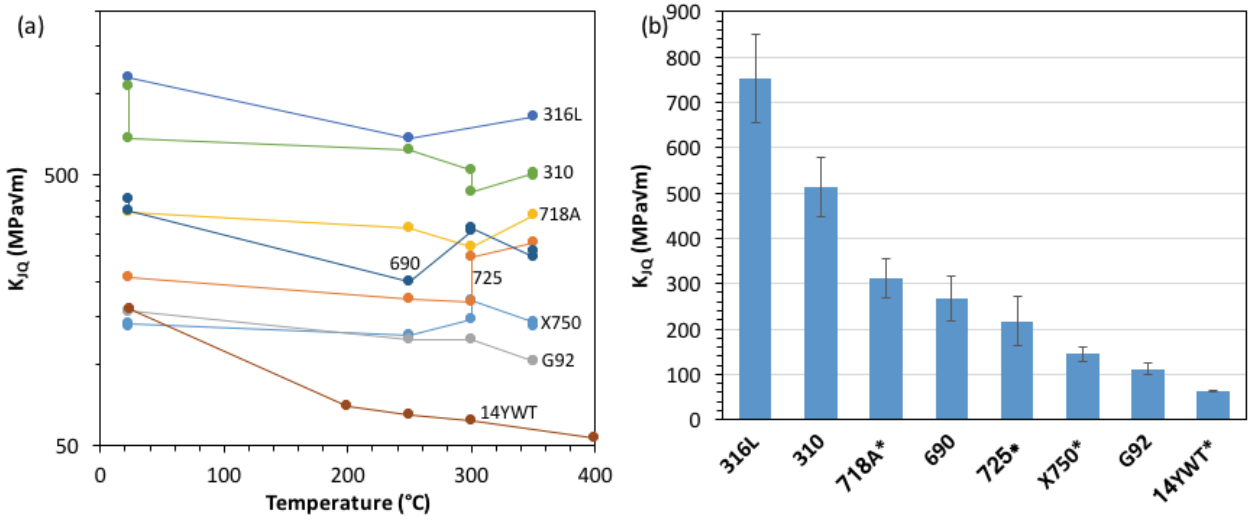

Figure 8. (a) Temperature-dependent fracture toughness and (b) averaged fracture toughness within 250-350°C for the tested alloys. (* high-strength alloys)

Tearing modulus (unitless) was also calculated from the slope of the linear fitting of the J-R curve between two exclusion lines times $E/[(\sigma_{YS}+\sigma_{TS})/2]^2$ with σ_{YS} and σ_{TS} as the yield and tensile strength of the material at each test temperature. Figure 9a shows the tearing modulus in logarithmic scale as a function of the test temperatures for the tested alloys. Similar to the major fracture toughness data in Figure 8a, the test temperatures did not result in significant changes in tearing modulus. By averaging the tearing modulus within 250–350°C, Figure 9b plots the average tearing moduli with standard deviations of the alloys at the LWR-relevant temperatures. Because of the limited statistic data, alloy 316L exhibited a much larger standard deviation than the other alloys. The results indicate that alloy 690 exhibited the highest tearing modulus on the order of 450. Austenitic stainless steels 316L and 310 showed somewhat lower tearing moduli on the order of 260. Ferritic alloy Grade 92 had a noticeably lower tearing modulus on the order of 70. The high-strength alloys 718A, 725, X750, and 14YWT had the lowest tearing modulus, ranging from ~45 to ~7.

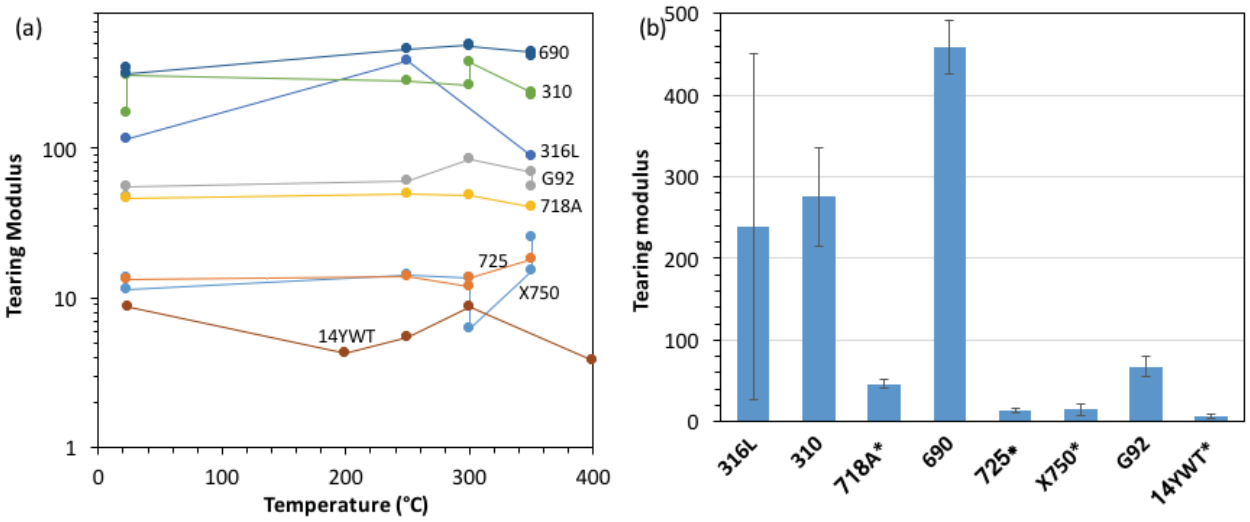

Figure 9. (a) Temperature-dependent tearing modulus and (b) averaged tearing modulus within 250–350°C for the tested alloys. (* high-strength alloys)

4. SUMMARY

Ductile fracture toughness of eight select advanced replacement alloys was evaluated at room temperature and the LWR-relevant temperatures around 300°C. The alloys include two ferritic alloys (Grade 92 and 14YWT), two austenitic stainless steels (316L and 310), and four Ni-base superalloys (718A, 725, 690, and X750). Compact tension specimens in 0.25T and 0.2T were machined from the alloys in the T-L and R-L orientations according to the product forms of the alloys.

Unlike the ferritic alloys showing slight decreases (Grade 92) or significant decreases (14YWT) in fracture toughness at elevated temperatures, the fracture toughness of the austenitic stainless steels and Ni-base superalloys were not strongly dependent upon the test temperatures. The fracture toughness of the alloys at the LWR-relevant temperatures was estimated by averaging the toughness values within 250–350°C, which indicated the fracture toughness of the alloys in a descending order as 316L (752±98 MPa√m), 310 (513±66 MPa√m), 718A (313±43 MPa√m), 690 (267±48 MPa√m), 725 (218±55 MPa√m), X750 (145±16 MPa√m), Grade 92 (112±12 MPa√m), and 14YWT (63±3 MPa√m).

Tearing modulus of the alloys was analyzed in the meantime, which were not strongly dependent upon the test temperatures. The high-strength alloys 718A, 725, X750, and 14YWT had the lowest tearing modulus, ranging from ~45 to ~7. Alloy 690 exhibited the highest tearing modulus on the order of 450, followed by 316L and 310 on the order of 260. Grade 92 had a noticeably lower tearing modulus on the order of 70.

REFERENCES

[1] E.A. Kenik, J.T. Busby, Radiation-induced degradation of stainless steel light water reactor internals, Mater. Sci. Eng. R 73 (2012) 67–83.

[2] F.A. Garner, Radiation damage in austenitic steels, in: R.J.M. Konings, T.R. Allen, R.E. Stoller, S. Yamanaka, Comprehensive Nuclear Materials, Elsevier, The Netherlands, 2012.

[3] L. Tan, R.E. Stoller, K.G. Field, Y. Yang, H. Nam, D. Morgan, B.D. Wirth, M.N. Gussev, J.T. Busby, Microstructural evolution of type 304 and 316 stainless steels under neutron irradiation at LWR relevant conditions, JOM 68 (2016) 517–529.

[4] Critical Issues Report and Roadmap for the Advanced Radiation-Resistant Materials Program, EPRI, Palo Alto, CA and the U.S. Department of Energy, Washington, DC: 2012. 1026482.

[5] L. Tan, B.A. Pint, X. Chen, Toughness and high-temperature steam oxidation evaluations of advanced alloys for core internals, ORNL/TM-2016/371.

[6] G.S. Was, M. Song, M. Wang, C. Lear, IASCC susceptibility and evolution of microstructure in austenitic alloys after proton irradiation, EPRI Report 2017, in preparation.

[7] L. Tan, B.A. Pint, High-temperature steam oxidation testing of select advanced replacement alloys for potential core internals, ORNL/TM-2017/228, May 19, 2017.

[8] X. Chen, R.K. Nanstand, M.A. Sokolov, E.T. Manneschmidt, Determining ductile fracture toughness in metals, Advanced Materials & Processes, 172 (2014) 19-23.